Size analysis of sub-resolution objects by Kerr microscopy

I. V. Soldatov,[1,2,a)] W. Jiang,[3,4] S. G. E. te Velthuis,[5] A. Hoffmann,[5] and R. Schäfer[1,6]
[1]*Leibniz Institute for Solid State and Materials Research (IFW) Dresden, Institute for Metallic Materials, Helmholtzstrasse 20, D-01069 Dresden, Germany*
[2]*Institute of Natural Sciences, Ural Federal University, 620002 Ekaterinburg, Russia*
[3]*State Key Laboratory of Low-Dimensional Quantum Physics, and Department of Physics, Tsinghua University, Beijing 100084, China*
[4]*Collaborative Innovation Center of Quantum Matter, Beijing 100084, China*
[5]*Materials Science Division, Argonne National Laboratory, Lemont, Illinois 60439, USA*
[6]*Institute for Materials Science, TU Dresden, 01062 Dresden, Germany*

(Received 3 March 2018; accepted 6 June 2018; published online 26 June 2018)

A Kerr microscopy method for the quantitative measurement of the size of magnetic objects that are smaller than the resolution limit is proposed. It can be applied to domain walls, bubble domains, and magnetic skyrmion-bubble hybrid microstructures. The method is based on the integral contrast, determined by proper line scans across the object, which turns out to be independent of the resolution of the microscope after normalization to the maximum domain contrast. *Published by AIP Publishing.* https://doi.org/10.1063/1.5027539

The size measurement of low dimensional magnetic objects such as domain walls, bubble domains, or skyrmions is important for fundamental and application-related research. If the object size is below the resolution limit of optical microscopy, sophisticated imaging techniques[1] like magnetic force microscopy, electron holography, polarized scanning electron microscopy, synchrotron-based X-ray microscopy, or Lorentz microscopy are required. Although providing high resolution, these methods are limited either in their applicability to dynamical experiments or in expense and complexity. Magneto-optical Kerr microscopy using visible light, on the other hand, is an in-house technique that offers high versatility without restrictions in imaging of dynamic processes, field compatibility, etc.[2–4] Recently, the method was utilized for the imaging of "skyrmionic" bubble domains with a size of several micrometers in metallic films with Dzyaloshinskii-Moriya interaction (DMI).[5,6] Skyrmion research, however, is interested in objects smaller than 100 nm, being below the resolution of optical microscopy that is 215 nm at best according to the Rayleigh criterion.[7] So, the question needs to be addressed to which extent Kerr microscopy can be applied to the imaging of sub-resolution-sized magnetic microstructures. Being encouraged by recent progress in digital Kerr microscopy,[8] which makes it possible to obtain pure in-plane contrast by using light emitting diodes (LEDs) in a pulsed mode as a light source, we have revisited a proposal by Pfannenmüller *et al.*[9] which uses 180° domain walls as calibration objects for the visibility of spin textures. In this paper, we have extended this method to two-dimensional objects and after its verification on magnetic bubble domains in films with perpendicular anisotropy, we have applied it to skyrmionic bubble hybrids with a size below the optical resolution.

When the size of an object is smaller than the wavelength of the light, diffraction effects due to the superposition of interfering light beams cannot be neglected as only few diffraction orders do contribute to image formation. Objects like domain walls may nevertheless be *visible* in a Kerr image, but with an apparent width that depends on the ratio of the true wall width to the resolution limit, given by the aperture of the objective lens and limitations of the camera. This diffraction broadening leads to a wall image that appears broader than the "true" width—the wall width can thus not be directly derived from the image. There is, however, a way to acquire the wall width quantitatively even in the case of walls with a real width below resolution by considering the *normalized integral intensity*.

Assume a 180° domain wall that separates two in-plane domains in a low-anisotropy magnetic material like iron or amorphous ribbons. The walls in such materials are vortex walls, derived from the asymmetric Bloch wall in thick magnetic films that have a vortex structure to avoid stray fields.[1] In bulk specimens, the vortices are confined to the surface neighborhoods, and right at the surface, the magnetization rotates in-plane in a Néel-like, one-dimensional way around the surface normal. In a Kerr image with sensitivity transverse to the domain magnetization, this Néel "cap" shows up as black or white line contrast depending on the rotation sense of the (surface) wall magnetization [see Fig. 1(a)], while the domain contrast vanishes. Optically, such a wall can be seen as a 180°-phase plate and the Kirchhoff diffraction theory[10] can be applied. According to this theory, which was extended by Wolter[11] for the case of one dimensional objects with a amplitude distribution determined by the object function $O(x)$, the amplitude of the light in the image plane is given by $B(x') = \int\int Q(\gamma)O(x)e^{2\pi i\gamma(x'-x)}dxd\gamma$. Here, x and x' are the coordinates across the wall with the origin in the wall center in the sample- and image plane, respectively, $Q(\gamma)$ is the pupil function, being constant within the aperture opening and zero outside; $\gamma = \sin\alpha/\lambda$ can be seen as coordinates in the aperture plane, with λ being the wavelength and α the angle at which the light leaves the objective lens with respect to the optical axis.

Before digital image processing was introduced,[12] Kranz and Buchenau[13] used a single value $B(0)$ to estimate

a)Electronic mail: i.soldatov@ifw-dresden.de

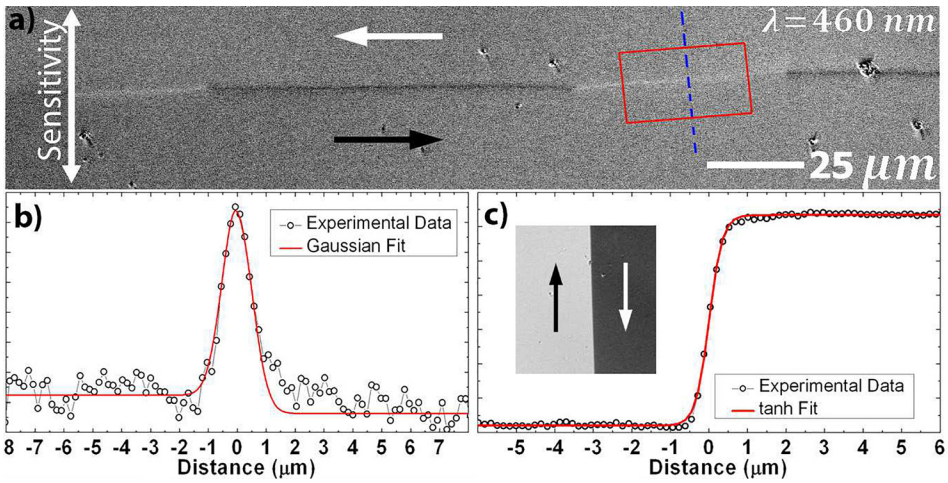

FIG. 1. (a) High-resolution Kerr image of a vortex wall on the (110)-surface of an Fe3%Si sheet (0.3 mm thick), imaged with a 100× oil immersion lens with a numerical aperture of 1.3. (b) Line scan across the wall (dots) with fit line, measured and averaged in the rectangular area indicated in (a). (c) Domain contrast after rotating the sample by 90°, providing the maximum "image intensity" under the given conditions.

the surface wall width on the bulk silicon iron material. Later, by considering a Gaussian profile for the wall contrast $O(x)$, Pfannenmüller[9,14] has shown that the integral light amplitude ($B_i = \int B(x)dx$), normalized to maximal possible amplitude $B(0)_{max}$, is independent of the pupil size, i.e., from the objective lens used. As the Kerr contrast is a linear function of magnetization, the integral wall *intensity* I_i is also independent of the pupil size, i.e., of the resolution of the optical instrument. For decreasing resolution, the wall image becomes simply wider but reduced in amplitude so that the integral stays constant. Thus, by measuring the domain wall intensity by a line scan across the wall [as in Fig. 1(b)], determining the integral of the intensity profile, and normalizing it to the maximum intensity I_{max} [Fig. 1(c)], it is possible to derive the integral domain wall width $w_i = I_i/I_{max} = \int I(x)dx/I_{max}$ that is independent of resolution.

In Fig. 2, this concept is verified for 180° vortex walls in an FeSi sheet and an amorphous ribbon. In Fig. 1(a), the walls were imaged in the longitudinal Kerr effect with sensitivity transverse to the domain magnetization by using blue LED light of 460 nm wavelength. Three objective lenses with different magnifications and numerical apertures (i.e., resolution) were employed as indicated in Fig. 2(a). Walls with segments of opposite surface rotation sense were deliberately chosen. By verifying equal integral intensities of both segment types, the superposition of magneto-optical diffraction effects arising from the surrounding domains, like the magnet-optical gradient effect,[15–17] are excluded. The typical intensity profile across a wall [as in Fig. 1(b)] was then approximated by the superposition of Gaussian- and tanh-functions, where the latter was used to compensate residual domain contrast. Then, the sample was rotated by 90° to obtain the maximum domain contrast [compare Fig. 1(c)] that is measured under the same illumination conditions. By integrating the line scan and normalizing it to the maximum contrast, the integral domain wall width w_i is obtained. Employing the three objective lenses, similar domain walls in the two materials were imaged [Fig. 2(a)], and their integral widths were determined and plotted as a function of the optical resolution limit [Fig. 2(b)]. The Rayleigh criterion, $r_{Rayleigh} = 1.22\lambda/2\text{NA}$ (NA is the lens numerical aperture), is the most appropriate criterion for optical microscopy as it takes into account not only the diffraction limit but also contrast considerations.[7]

As expected, the derived wall width is independent of the resolution within experimental error. Even at the lowest resolution of 560 nm (20× lens), a wall with a width of just 130 nm, which is only ~23% of the resolution, can be quantitatively visualized. Extrapolating this fact to the [100×/1.3] lens with the highest resolution of 215 nm, a visibility of walls that are just ~50 nm (23% of 215 nm) wide can be expected. Note that this "visibility limit" is a conservative number. Vortex walls, as discussed here, require the longitudinal Kerr effect at oblique light incidence due to their in-plane surface magnetization. For small NA objectives, the obtainable in-plane contrast is very weak.[4] Only for the highest magnification lenses, it is possible to get close to the maximum longitudinal Kerr contrast, which, nevertheless, is ten times weaker than the polar contrast.[2] If perpendicularly magnetized objects like nanowires are imaged under polar

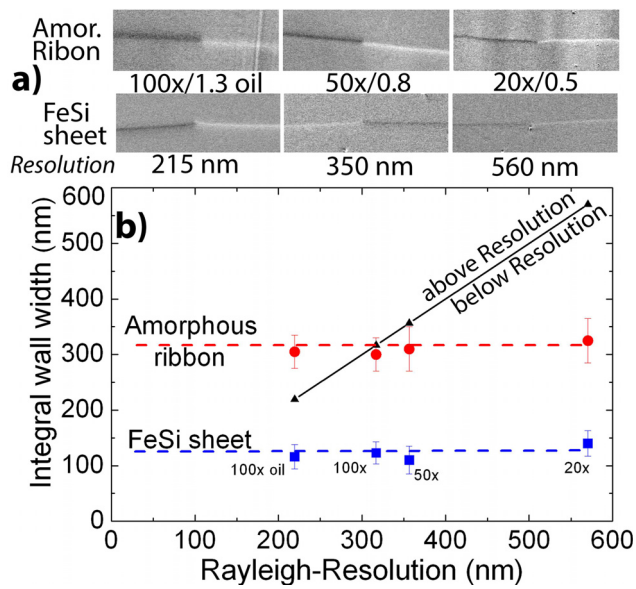

FIG. 2. (a) Kerr images of vortex walls on an amorphous $Fe_{24}Co_{18}Ni_{40}Si_2B_{16}$ ribbon (20 μm thick, with well-ordered domain walls due to an induced anisotropy—*sample courtesy G. Herzer, VAC*) and on the (110)-surface of an Fe3%Si sheet of 0.3 mm thickness. Three objective lenses with magnification/numerical aperture and resolutions as indicated were used. (b) Integral wall widths as a function of resolution for the two materials. Each data point represents an average of 5 to 7 independent measurements. The black line represents the resolution of the objective lens with objects of size above the line can be resolved and of size below the line are too small to be resolved.

conditions, i.e., at perpendicular light incidence, a visibility of magnetic contrast can be expected even for wire widths well below 50 nm.

At oblique light incidence, there is always a superposition of longitudinal and polar Kerr effects,[3] i.e., of sensitivities to in- and out-of-plane magnetization components. In Ref. 8, we have shown that *pure* in-plane sensitivity can be obtained by processing the illumination in a proper way, which at the same time leads to a doubling of the in-plane contrast and thus an improved sensitivity. Although a reduction of the experimental error in the wall width measurement is to be expected in this mode, a noticeable improvement could not be observed (not shown). Nevertheless, the use of pure in-plane sensitivity eliminates the necessity of 90° sample rotation to get the maximal contrast for the integral intensity normalization. Instead, saturation in the sensitivity direction in an external magnetic field can be applied as in the pure in-plane mode, and all polar contributions, including those which may arise from the Faraday effect in the lenses, are suppressed.[8,18]

Different from domain walls, *skyrmion* research aims at two-dimensional objects, for which the above theory can be easily adapted, however, by substituting the intensity distribution $I(x)$ across the wall by a 2D distribution $I(x, y)$ with subsequent integration $\int\int I(x,y)dxdy$. After normalization to the maximal contrast, the *integral area* of the object $A_i = I_i/I_{max} = \int\int I(x,y)dxdy/I_{max}$ is obtained. If the magnetic domain on the surface has a circular symmetry of diameter D, its characteristic size can finally be derived as $D_i = \sqrt{4A_i/\pi}$.

A model system for the experimental verification of this concept is YIG (Yttrium Iron Garnet) films with strong perpendicular anisotropy. Driven by the magnetodipolar interaction and depending on the magnetic field history,[1] such films display bubble- or band domains at zero field [Fig. 3(a)] which are homogeneously magnetized along the easy axis and that are separated by narrow 180° walls of (predominant) Bloch character. Being several micrometers wide, those domains are resolved with a variety of objective lenses (see below). They can thus be used to obtain the maximal contrast I_{max}. In the perpendicular magnetic field, a lattice of isolated bubbles is formed [Fig. 3(b)] that shrink in size with the increasing field [Fig. 3(c)] until they collapse. The images in Figs. 3(a)–3(c) were obtained by using red LED light with a 640 nm wavelength for maximum magneto-optical rotation[19] and the highest-resolution [100×Oil/1.3/300] objective with (magnification/NA/Rayleigh resolution in nanometer). With this lens, the bubbles can be fully resolved up to the collapse field as their size is far above the resolution of 300 nm. This can be seen from the inset in Fig. 3(d). Here, two bubble size distributions are plotted, obtained by means of both integral and "visual" techniques, where the "visual size" was determined from the full width at half maximum (FWHM) of each intensity scan across the bubble. Both methods lead to the same average bubble size of $D = 1.05 \pm 0.05\ \mu$m. If the domains were not resolved, the visual width would be larger than the integral width.

The bubbles close to collapse were then imaged by employing a number of objective lenses with different resolutions: [100×Oil/1.3/300], [50×/0.8/488], [20×/0.5/780],

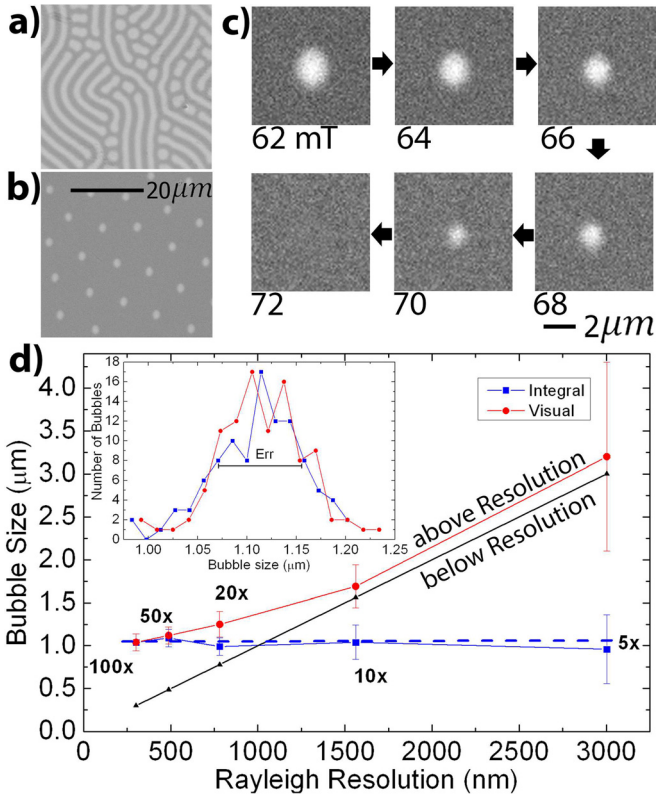

FIG. 3. Kerr images of mixed band- and bubble domains (a) and isolated bubbles (b) in a micron-thick YIG film with strong perpendicular anisotropy, imaged in red LED light by using a [100×Oil/1.3/246] objective lens. (c) Evaluation of a bubble in the increasing perpendicular field up to its collapse. (d) Integral and visual (full width at half maximum) bubble size close to the collapse field as a function of Rayleigh resolution. The inset shows the bubble size distributions (integral and visual) close to collapse, imaged with the 100× lens. The black line represents the resolution of the objective lens used.

[10×/0.25/1561], and [5×/0.13/3000]. The size of all bubbles appearing in each image (up to 30 domains for high- and up to 500 for low magnification lenses) was derived by means of both integral and "visual" techniques and is plotted as a function of Rayleigh resolution in Fig. 3(d). Both methods give an identical bubble size for the 100× and 50× lenses as the domains size is above the resolution limit for both objectives. For the 10× and 5× lenses, for which the bubble size is clearly below the resolution limit, the integral bubble size is still correct as it coincides with that obtained with the high magnifying lenses, while the visual observation provides overestimated values. In the case of the 20× lens, although the optical resolution should be sufficient for accurate measurements, the visual size already deviates from the true value. This could be associated with the reduction of the effective aperture of an objective lens due to an illumination spot in the center of the back focal plane as recently shown by Ogasawara *et al.*[20] Thus, the real optical resolution of the apparatus could be worse than that estimated by the Rayleigh criterion. In our case, the resolution is completely determined by microscope optics as no pixel binning in the CCD camera was used.[4] Anyway, as in the case of the vortex walls, the derived integral bubble size turns out to be independent of the aperture within experimental error, and the integral method, originally developed for 1D optical structures, can be fairly applied for quantifying 2D objects.

Even a resolution of 3 μm (5× lens) is still sufficient to characterize bubbles with a size of 1 μm, which is just 30% of the visible resolution.

The "classical" bubble domains in YIG, discussed so far, can still be resolved by using high-aperture objectives—for this paper, the resolution was *deliberately* reduced for demonstration purposes only. Magnetic objects that are truly smaller than the ultimate resolution limit can be found in multilayered metallic films with interface-induced DMI and moderate perpendicular anisotropy.[21] If the DMI is sufficiently strong, a homo-chiral domain wall structure is favored that leads to bubble domains with extended domain walls of Néel character,[22] i.e., to bubbles with extended areas of inhomogeneous surface magnetization. When getting smaller, the bubbles approach the magnetization profile of chiral skyrmions.[23] In fact, there is no sharp boundary between chiral skyrmions formed under the influence of chiral interactions (DMI) and bubble domains stabilized by the surface demagnetization effects,[24] so that these objects, which are actually stabilized under both interactions,[25] may be called "bubble-skyrmion hybrids." The inset to Fig. 4 shows such hybrids in a [Pt/Co/Ir]Pt multilayer, imaged at the highest attainable resolution of $r_{Rayleigh} = 215$ nm (100×/1.3 Oil immersion lens, blue light with 460 nm wavelength). Spots of different intensities are observed, representing hybrid domains of different sizes. The darkest spots are well-resolved bubbles, which can be used for contrast normalization. The latter can be alternatively derived from magnetization loops in the perpendicularly applied field.

Assuming—as a first approximation—a homogenous surface magnetization and applying the same procedure as for the bubbles in YIG, the integral and visual sizes of the hybrid domains were analyzed and are plotted in Fig. 4 as a function of the integral object size considered as *"true."* Apparently, in that case, the integral size distribution shows a linear dependency with a slope of one. The visually estimated bubbles, if they are bigger than ~300 nm, fall on the same curve. However, with the decrease in the domain size, their average visually estimated diameters [solid curve in Fig. 4(b)] do not follow the integral curve but rather approach a constant value of around 250 nm close to the optical resolution of the system.

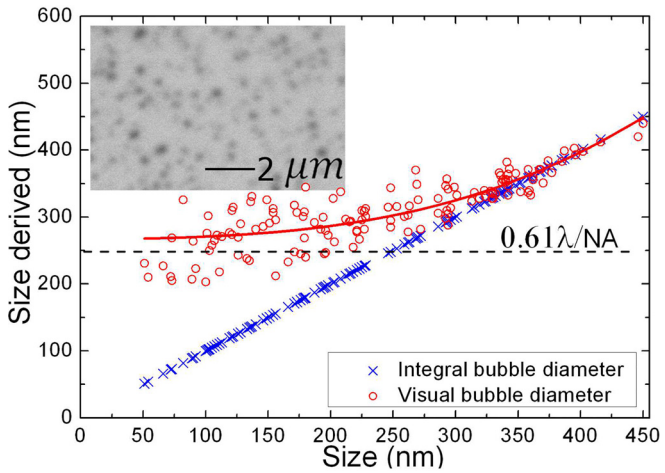

FIG. 4. Integral (blue dots) and visual (red dots) bubble size as a function of integral bubble size, considered as "true." The red curve shows the mean average of the visual bubble size. The inset shows the Kerr image of skyrmion-bubble hybrids in [Pt/Co/Ir]Pt multilayer [Si substrate/Ta(2 nm)/[Pt(1.5 nm)/Co(1 nm)/Ir(1 nm)]×5/Pt(2 nm)] in the zero field with the 100× lens.

By assuming a smooth, skyrmion-like rotation of magnetization, which can be described by a Gaussian profile of the polar magnetization component, the integral technique to determine the object width can nevertheless be applied: If the *real* Kerr contrast profiles (that follow the magnetization profile precisely) of hybrid objects and classical bubbles, both with dimensions well below the resolution limit, are convoluted with the optical transfer function of the microscope (which is estimated for the highest magnification to be around 200 nm in our case) and their resulting contrast profiles are almost the same, then the FWHM of the Gaussian hybrid is only around 15% smaller than that of a classical bubble (not shown).

In summary, a method for the quantitative measurement of the size of domain walls, bubble domains, and magnetic skyrmion-bubble hybrid microstructures that are smaller than the optical resolution limit has been developed. It is based on the integral contrast, determined by proper line scans across the object. By normalization to the maximum domain contrast, the integral object width turns out to be independent of the resolution of the microscope. This integral method was tested on one-dimensional vortex domain walls, then extended to two-dimensional objects, and verified on classical bubble domains in the garnet material. In a first attempt, the approach was used for the integral size determination of skyrmion bubble hybrids in a [Pt/Co/Ir]Pt multilayer with a size down to three times smaller than the resolution limit. The integral method can also be applied to magnetic objects with asymmetric magnetization and thus intensity distributions (like asymmetric Bloch walls, see Ref. 9), whereas irregularities (like bulges in 2D-objects) will have an influence on the accuracy of the obtained object size. The method cannot be applied to objects that are closer together than the Rayleigh limit. The maximum Kerr contrast, to which the integral contrast is normalized, can most reliably be determined by adjusting domains of sufficient size as shown in this article. If this is not possible for physical reasons, the maximum contrast can still be measured by saturating the sample in strong applied fields of proper directions and by eliminating parasitic Faraday contributions arising in the objective lens, either by applying the pure in-plane imaging mode[8,18] in the case of in-plane media or by using a motorized analyser for perpendicular media.[26] The method can be easily adapted to any imagining technique, applied to objects of known shape and for which the observed contrast can be normalized.

We thank Alexei Bogdanov (IFW), Dmitry Berkov (GNRL Jena), and Jens Ehrig (TU Dresden) for helpful discussions and Kornelius Nielsch (IFW) for support. Work at Argonne National Laboratory was supported by the U.S. Department of Energy, Office of Science, Materials Sciences and Engineering Division ([Pt/Co/Ir]Pt sample design and growth).

[1]A. Hubert and R. Schäfer, *Magnetic Domains: The Analysis of Magnetic Microstructures* (Springer, New York, 1998), p. 696.
[2]W. Kuch, R. Schäfer, P. Fischer, and F. Hillebrecht, *Magnetic Microscopy of Layered Structures* (Springer, New York, 2015), p. 246.

[3]R. Schäfer, "Investigation of domains and dynamics of domain walls by the magneto-optical Kerr-effect," in *Handbook of Magnetism and Advanced Magnetic Materials* (John Wiley & Sons, Ltd, 2007).
[4]J. McCord, J. Phys. D: Appl. Phys. **48**, 333001 (2015).
[5]W. Jiang, P. Upadhyaya, W. Zhang, G. Yu, M. B. Jungfleisch, F. Y. Fradin, J. E. Pearson, Y. Tserkovnyak, K. L. Wang, O. Heinonen, S. G. E. te Velthuis, and A. Hoffmann, Science **349**, 283 (2015).
[6]J. Wanjun, X. Zhang, G. Yu, W. Zhang, X. Wang, M. B. Jungfleisch, J. E. Pearson, X. Cheng, O. Heinonen, K. L. Wang, Y. Zhou, A. Hoffmann, and S. G. E. te Velthuis, Nat. Phys. **13**, 162 (2017).
[7]R. Wayne, *Light and Video Microscopy* (Elsevier, Netherlands, 2014), p. 368.
[8]I. V. Soldatov and R. Schafer, Rev. Sci. Instrum. **88**, 073701 (2017).
[9]J. Pfannenmüller, W. Rave, and H. Alex, in *12th International Colloquium on Magnetic Films and Surfaces*, Le Creusot (1988), pp. TP–14.
[10]M. Born and E. Wolf, *Principles of Optics* (Cambridge University Press, 1999), p. 952.
[11]H. Wolter, "*Schlieren-, Phasenkontrast-Und Lichtschittverfahren*" in *Handbuch Der Physik*, edited by S. Flügge (Springer, Berlin, 1956), pp. 589–603.
[12]F. Schmidt, W. Rave, and A. Hubert, IEEE Trans. Magn. **21**, 1596 (1985).
[13]J. Kranz and U. Buchenau, IEEE Trans. Magn. **2**, 297 (1966).
[14]J. Pfannenmüller, Ph.D. thesis, Technical Faculty of University Erlangen-Nürnberg, 1988.
[15]R. Schäfer and A. Hubert, Phys. Status Solidi (a) **118**, 271 (1990).
[16]R. Schäfer, M. Rührig, and A. Hubert, Phys. Status Solidi (a) **145**, 167 (1994).
[17]R. Schäfer, C. Hamann, J. McCord, L. Schultz, and V. Kambersky, New J. Phys. **12**, 053006 (2010).
[18]D. Marko, I. Soldatov, M. Tekielak, and R. Schäfer, J. Magn. Magn. Mater. **396**, 9 (2015).
[19]L. E. Helseth, R. W. Hansen, E. I. Il'yashenko, M. Baziljevich, and T. H. Johansen, Phys. Rev. B **64**, 174406 (2001).
[20]T. Ogasawara, Jpn. J. Appl. Phys., Part 1 **56**, 108002 (2017).
[21]S. Woo, K. Litzius, B. Krüger, M. Y. Im, L. Caretta, K. Richter, M. Mann, A. Krone, R. M. Reeve, M. Weigand, P. Agrawal, I. Lemesh, M. A. Mawass, P. Fischer, M. Kläui, and G. Beach, Nat. Mater. **15**, 501 (2016).
[22]A. Thiaville, S. Rohart, E. Jué, V. Cros, and A. Fert, EPL **100**, 57002 (2012).
[23]A. N. Bogdanov and D. A. Yablonskii, Zh. Eksp. Teor. Fiz. **95**, 178 (1989), http://www.jetp.ac.ru/cgi-bin/e/index/r/95/1/p178?a=list.
[24]N. S. Kiselev, A. N. Bogdanov, R. Schäfer, and U. Rössler, J. Phys. D: Appl. Phys. **44**, 392001 (2011).
[25]A. Bogdanov, private communication (21 March 2017).
[26]I. V. Soldatov and R. Schafer, J. Appl. Phys. **122**, 153906 (2017).